2/2016
an/year XXV
ISSN 1453-0392
Sudarea şi Încercarea Materialelor

WELDING & MATERIAL TESTING

bid ISIM
Buletinul Institutului Naţional de Cercetare-Dezvoltare în Sudură şi Încercări de Materiale - ISIM Timişoara, România

bid ISIM 2/2016 Year XXV

bid-ISIM –
Welding and Material Testing

acknowledged by CNCSIS,
B+ journals category,
quarterly review
ISSN 1453-0392
www.bid-isim.ro

Edited by

ISIM Timişoara

30, Mihai Viteazu Bv.
300222 Timişoara, România
Tel.: +40 256 491830
E-mail: isim@isim.ro
www.isim.ro

Prepress & Printing

Tempus

24 Nufăr Str.
300169 Timişoara, Romania
Tel./fax: +40 256-226001

contents

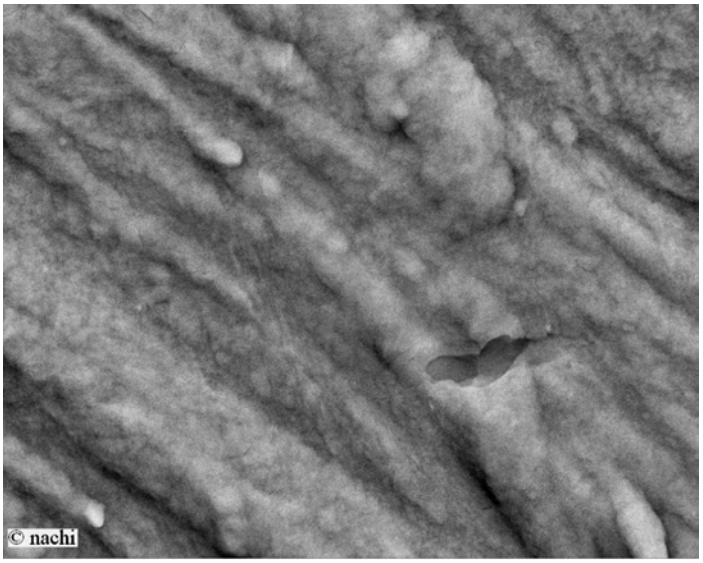

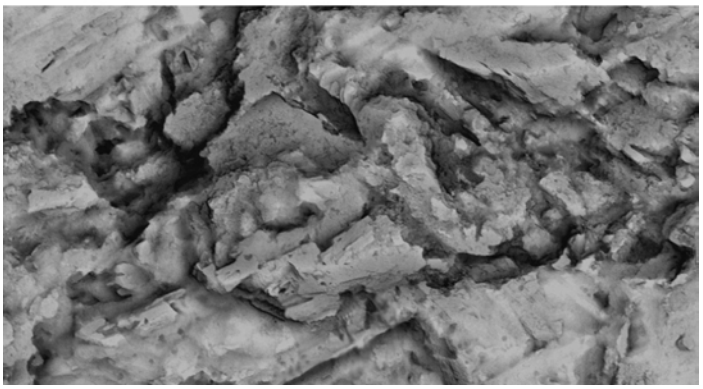

Sudarea şi încercarea Materialelor

ABSTRACTS

Seismic strengthening of masonry using some advanced composite materials

C.S. Dragomir, D. Dobre, E.S. Georgescu

The seismic vulnerability of masonry buildings may be reduced through the increasing of strength and rigidity by reinforcement or confinement. In order to support the provisions of Romanian codes, some modern manufacturing technologies have produced a lot of new composite building materials. The paper presents the theoretical basis of reinforcing masonry with polymer grids and the results of experimental and numerical analysis research on a 3D masonry model with the mechanical performance enhanced by the reinforcement polymer grids.

Prediction of stress distribution of pressure vessel shell using numerical simulation

M. Prvulovic, M. Ristic, S. Budimir, M. Prokolab, Z. Milutinovic

In this paper, a comparative analysis of stresses in the pressure vessel shell, using a numerical simulation in software package CATIA and analytical calculation has been represented. Material of the pressure vessel is stainless steel 304L, and it is intended for substances storing, that have corrosion effect.

Using the finite element method it was performed a modeling of the pressure vessel for a real geometry, where it has been considered a shape of shall and geometry of connections, supports and welded joints, because they might be places for the occurrence of stress concentration.

Based on the analysis results, the highest achieved stresses are in the torus part of the head and around the connections. It was observed a good accordance between the results obtained on the basis of analytical strength calculation, and results of numerical simulation. Shown methodology might have application of stress prediction in the similar industrial equipment.

Spot weld growth on medium carbon steel. Part 2: Servo based electrode actuation system

Nachimani Charde

In the part 1 of this research, the medium carbon steel was welded using pneumatic based electrode actuation system and subsequently it was investigated for the fatigue strength under tensile shear load, hardness and micro structural changes. Similar type of welding conditions and strength tests were conducted in this experiment but the electrode actuation system was replaced by servo based electrode actuation system; instead. A 1.5 kW powered-servo motor and its driving mechanical assembly were electro-fitted as to improve the force profiles before, during and after the welding process takes place. In doing so, the force exertions are systematically distributed and the corresponding changes are analyzed for the welds improvements. As such the specimen sizes and corresponding alignments were kept constant that of the previous experiments had but the welding lobe parameters and force presets were slightly calibrated for. The servo based electrode actuation system improves the electrically generated forging forces during welding process and consequently minimizes the porosity occurrences at the welded region. Specifically the diameters of fused regions were increased for the same welding conditions as compared to part 1 results and therefore the tensile loading force was significantly increased to break the welded joints in this part. However the hardness distributive values were remained approximately the same as compared to the first part because the solidification process is seemed to be happened for the duration. This has been confirmed by the metallurgical study which has revealed that the micro structural orientation in similar fashion for both experiments.

Spot weld growth on medium carbon steel. Part 2: Servo based electrode actuation system

Nachimani Charde

Department of Mechanical Engineering, Faculty of Engineering, University Malaya, Malaysia

E-mail: nachicharde@yahoo.com

Keywords

Medium carbon steel, Carbon steel welding, Spot welding of steel, Electrode actuation.

1. Introduction

Force changes during the entire welding process are important parameter to understand as it diminishes the quality of welded regions in terms of fatigue strength. When the pneumatic based and servo based electrode actuation system are separately analyzed, it noticeably varies from the force profiles distribution, particularly at the increment of forging forces during weld cycles [1]. These forging forces are irremovable properties as it was induced due to the high AC current flow. As the welding current movement goes on both direction (positive to negative on half cycle and vice versa) during welding process in AC spot welder; the forging forces do exist significantly in electrical means [2]. This effects, of course, can be reduced by using servo based electrode actuation system with supportive braking system. Literally, the servo based system squeezes the base metals very smoothly and locks the mechanical lever using brakes once it reaches the exact pressing force levels [3]. So the strong hold of base metals during weld cycles have resulted low generation of forging force effect and hence the heat diffusion is significantly improved

Figure 1 and 2 are showing the force profiles of medium carbon steels when welded with pneumatic and servo-based electrode actuation systems, respectively [4].

2. Experimentation

The entire research was carried out using 75 kVA spot welder, powered by AC waveform and capable of handling up to 99 weld cycles in whole. Each cycle consumes 0.2 mS in time scale. Pre and post welding mechanism was available but only single welding current and single welding force (SISF) method was taken into consideration for this paper. The base metals were prepared in rectangular shape metal sheets (200 mm x 25 mm x 2 mm) as used in part 1 before and it has been shown in Fig. 1. The chemical properties are: C = 0.40; Cu = 0.016; Mn = 0.90; P = 0.040; S = 0.050 and Si = 0.006 for medium carbon steel. Hardness was 65 HRB when measured with Rockwell hardness tester on scale 'B' and the truncated-electrode tip was 5 mm diameter which was selected from RWMA's class two (copper and chromium) category.

A pair of test sample was initially placed on the top of lower electrode (tip) of the welder as overlaying 60 mm on each other in lap-joint fashion and then the initiating pedal was pressed. The upper electrode was located at the home position and once the welding process starts, the electrode moves (400 rpm) from home position to base metals' close position with reversed maximum torque. The reverse torque minimizes the position errors of the 50 kg of electrode assembly in free fall. When it

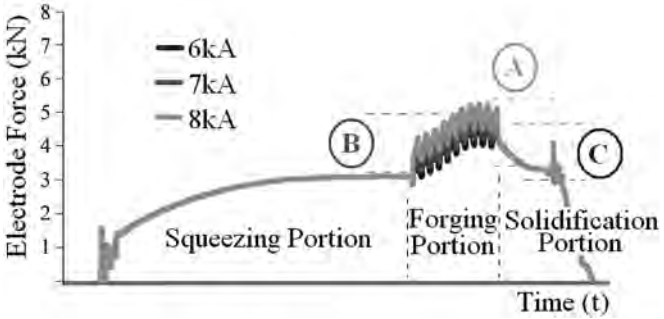

Figure 1. Force profiles of pneumatically driven system for medium carbon steel.

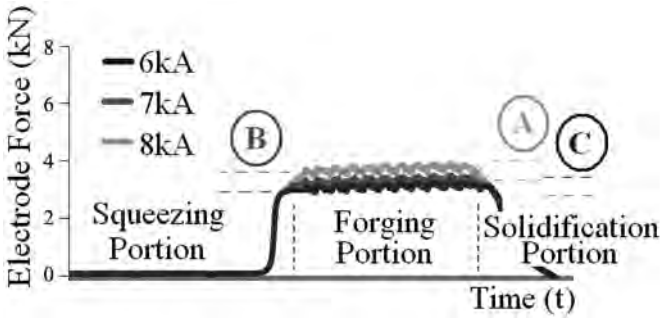

Figure 2. Force profiles of servo driven system for medium carbon steel.

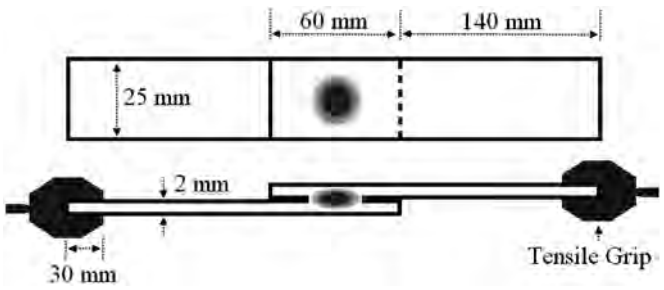

Figure 3. Test sample.

reaches the point 'A', the electrode movement is electrically slowed (50 rpm) as to produce smooth touch between electrodes to sheets. This movement would last until the present value of

force is obtained. When the required force value is achieved; then the electrode movement will be stopped and also locked with the aid of braking systems of servomotor. So that the electrode lever assembly becomes constantly-fixed mechanical arm in this set up. Thereafter the welding current will be released and hold it firmly for the solidification process. After the cold work is over, the braking system releases the lock and the upper electrode lever moves back to its home position as shown in Figure 4. These sequential movements are generated through a computer program from Schneider Electrics and in doing so, the forging forces are significantly controlled. Technically, 30 cycles for squeezing, 10-20 cycles for welding current delivery and 20 cycle for solidification process were followed in continuous order. Figure 4 shows the electrode movement using few linear PIDs.

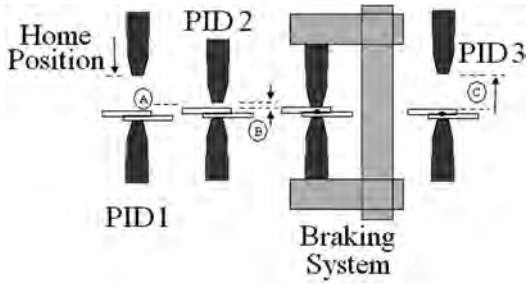

Figure 4. Electrode movement of servo based system.

Table 1. Weld schedule (welding current and welding time-variations).

Sample No	Weld Schedule	Electrode Tip	Time [cycle]	Current [kA]	Force [kN]
1-7	1	5	10	6	3
8-14	2	5	10	7	3
15-21	3	5	10	8	3
22-28	4	5	15	6	3
29-35	5	5	15	7	3
36-42	6	5	15	8	3
43-49	7	5	20	6	3
50-56	8	5	20	7	3
57-63	9	5	20	8	3

Table 2. Weld schedule (welding current and electrode force-variations).

Sample No	Weld Schedule	Electrode Tip	Time [cycle]	Current [kA]	Force [kN]
1-7	1	5	10	6	3
8-14	2	5	10	7	3
15-21	3	5	10	8	3
22-28	4	5	10	6	4.5
29-35	5	5	10	7	4.5
36-42	6	5	10	8	4.5
43-49	7	5	10	6	6
50-56	8	5	10	7	6
57-63	9	5	10	8	6

The welding conditions that were followed for the entire welding process is shown in table 1 and 2. This table is exactly followed from part 1 of this research as to distinguish the improvements that made by servo based electrode actuation system. Assessments of the bonded-strength of welded pairs were carried out using 100 kN tensile testing machine. The cross head speed was maintained at 70 mm per minutes and the metal sheets were held for 30 mm tensile grip out of 200 mm original length as shown in Figure 3. The ultimate tensile strength (UTS) was measured as the maximum weld strength after which the welded sample will crack itself. An average strength value of the five samples for each weld schedule was taken as final values of that particular weld schedule. The hardness test was carried out using a Rockwell hardness tester applying scale 'B' with twenty kilogram of pressing force. Twenty two points were measured from left hand side of base metal through the welded areas and ended at the right hand side of base metal. The welded samples for the medium carbon steel were cut at the line of its diameter and mounted it using resin powder on hot press mount-machine. The mounted samples were roughly polished using silicon papers 1200/800p and 600/200p and also continuously further polished using Metadi polishing cloth with suspension liquid of 0.05 and 0.04 micron. This polishing process has been conducted about thirty minutes to one hour on each sample until the shining surfaces were seen. The well-polished samples were later kept in nitrogen-filled chamber to reduce the oxidation effects before taking into the SEM scanner. At last the ferric chloride (500 ml for 10 samples) was used to etch these well prepared samples in a pot about 30-45 minutes. After that the samples were rinsed off using plain water and dried using air blower. It was sent to SEM scanning procedures without any delay because the carbon steels are very sensitive to atmospheric moisture.

3. Result and Discussion

3.1. Tensile shear test results

The tensile-shear test (Figure 5) was carried out using hundred kilo Newton (100 kN) capacity machine to determine the strength of spot welded samples of both (current versus weld time; current versus force) sets [5]. Average strength values from the five samples were taken as the equivalent

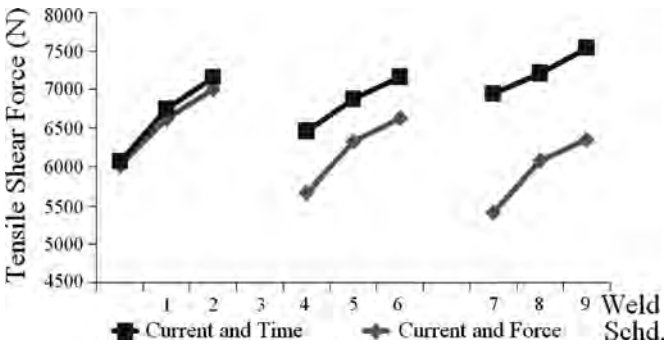

Figure 5. Tensile shear test results.

strength of that particular weld schedules as how I did in part 1. As for the weld schedules from 1 to 2 and 2 to 3 are analyzed; the loading force increment was noticed due to the increment of welding current from 6 to 7 and 7 to 8 kA respectively.

Noticeably there are increments in shear force as compared to pneumatic based tensile test results which presented in part 1 of this research. The additional increments are also noticed for the following weld schedules of 4, 5 and 6 as well as 7, 8, and 9. This obviously states that increase in current has caused increase in loading force due to the increase in diameters regardless of electrode actuation systems. Similar results are also found for the weld time increment but the diameters seem to be wider in servo based system than the pneumatic based system.

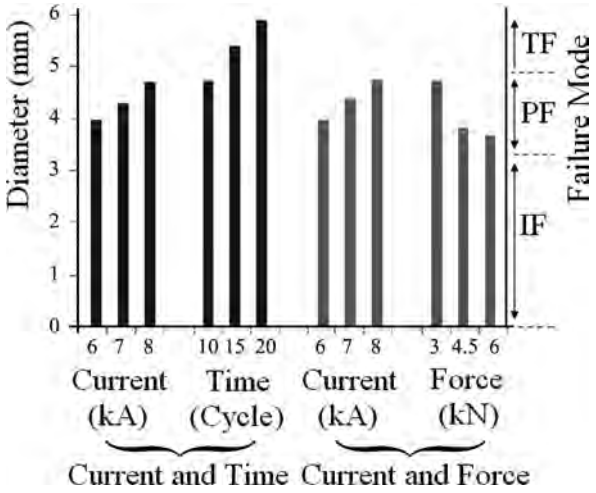

Figure 6. Diameters of weld nuggets and failure modes of tensile test

The Figure 6 shows the diameters changes with respect to current; weld time and force changes. This current increment is found in both set of attempts. When the current and weld time incremental set is considered: the weld time is also increased the shear force because it increases the diameters and resulting strong bonds between base metals. When the diameters of welded samples are considered for servo based experiments; it is obviously seen from Figure 6 that it has increased the bead width and it did not produce any interfacial failure at all [6]. Furthermore the force reduction was not affected the weld bead very much as compared to pneumatic based diameters' results [7]. Furthermore, when the force from 3 to 4.5 and 4.5 to 6 kN are considered; the shear force is slightly reduced because the resistive components were reduced in the heating process which is an important proportional coefficient of heat formula ($Q=I^2Rt$) [8-9].

3.2. Failure modes

Having considered the crack initiation of tensile test (Figure 7) under servo based electrode actuation system; only the button-pullout crack initiation was noticed throughout the experiment [10,11]. However when the post crack propagation direction is considered to analyze further; then two type of modes were consequently observed. Firstly the crack initiation starts from any side of base metal at the heat affected areas and resulting complete tear of base metal on one side. This sort of failure is called as partial fracture (PF) when post crack propagation mode is considered. Secondly the crack initiation starts from both sides of base metal simultaneously at the heat affected areas and resulting tear of base metal on both sides. This sort of failure is called as perfect fracture (TF) and also known to be best weld joint.

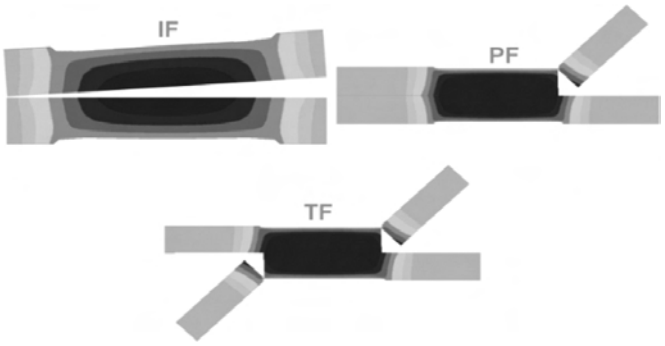

Figure 7. Crack initiation and post crack propagation.

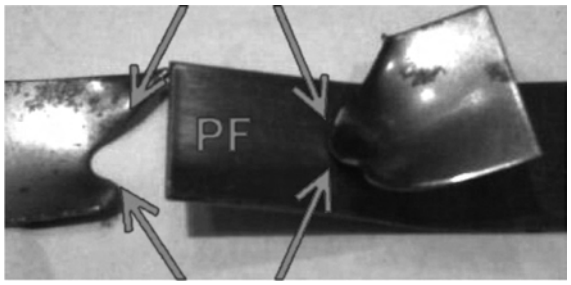

Figure 8. Tear from one side (PF).

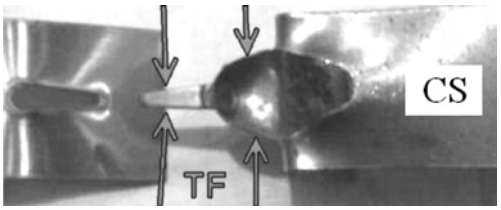

Figure 9. Tear from either side or button pullout (PF).

In this experiments, the interfacial fracture was not seen anywhere of the weld schedule. Figure 8 and 9 are showing the post crack propagation of servo based welded samples. The PF failure mode's shear force was observed between 5.5 to 7.2 kN while the TF failure mode's shear force was observed above 7.2 kN. Figure 6 shows the obvious relationship between weld diameters and corresponding failure modes that obtained for servo based electrode actuation system.

3.3. Hardness test results

As for the hardness test, the fusion zones (FZ) seem to be symmetrical weld joints and oval shape in overall as how it was appeared in the pneumatic based system[12-13]. It has been hardened at the welded areas by the means of solidification process and the fused areas are directly related to the thermal expansion's rate (12×10^{-6} K^{-1}) of medium carbon steel. Meanwhile the heat affected zones' (HAZ) hardness was slightly lower than the fusion zone but higher than the base metals as how Kent et al (2008) was reported in his research. It is very clear that the oval shape of heat affected zones was noticed due to the 30 degree-truncated electrodes tips and also due to the thermal conductivity rate (54 W m^{-1} K^{-1}) of medium carbon steel. The hardness was measured for all the nine weld schedules (Figure 10) and plotted against the three major regions of samples for servo based system. The hardness values of unwelded areas were around 55 HRB; the

fusion zones were around 110 HRB and the heat affected zones were approximately 90 HRB. The hardness results were not significantly changed as compared to pneumatic based system because the solidification process determines the hardness of

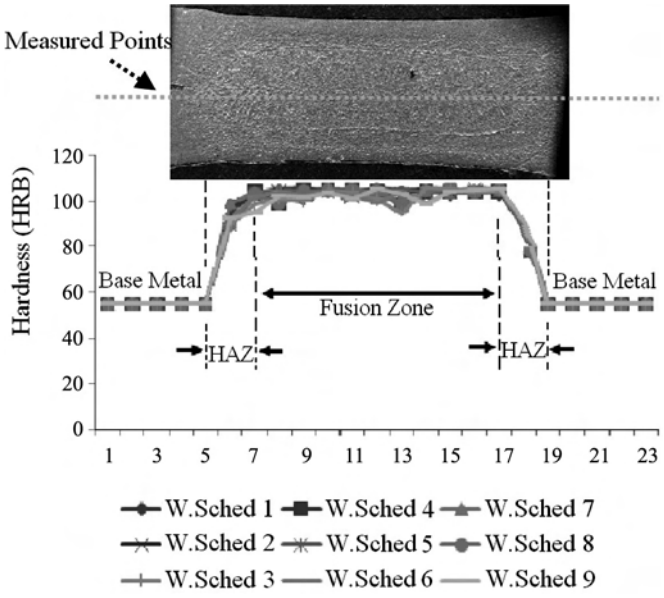

Figure 10. Hardness of medium carbon steels (servo based).

welded zones for both the pneumatics based systems and the servo based system. The time consumed for the solidification process on the pneumatic based system is equal to the time that of the solidification process by the servo based system. As such there is no noticeable change in hardness distribution for both electrode actuation systems.

3.4. Metallurgical study

A similar method for the micro structural observation was performed to study the changes during cold work in the servo-based welded samples [14-15]. Although the procedures were same, there are no big differences were seen in micro structural granular matrix except the diameter, itself. The diameters of

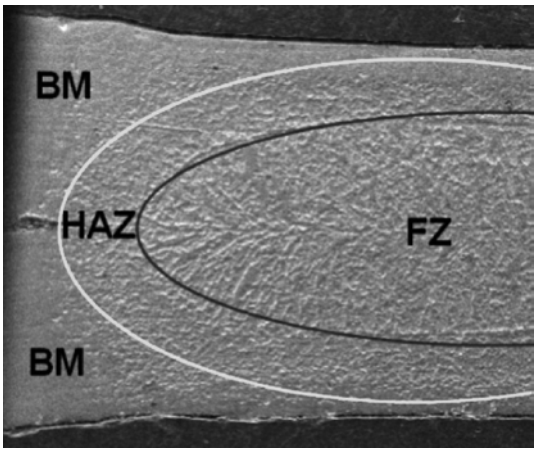

Figure 11. Structural zones.

the welded areas of servo-based system were wider than the pneumatic-based welded samples. So it is very clear that; when the forging force is reduced, the weld diameter is increased. Figure 11 shows the fundamental zones that categorized for weld nuggets.

The base metals' micro structures have more pearlite structure than the ferrite strand in its original region (Fig. 12) as how it was made about with larger grains as compare to the other two zones. The heat affected zones are transformed into partial pearlite phases with some areas of pearlite and ferrite patches (Fig. 13) with refined grains. However the fusion zones (Fig. 14) were seemed to be encapsuled with smaller grain strands as compare to the other two regions. This region has highest pearlite and ferrite patches formation with very clearer areas of ferrites strands.

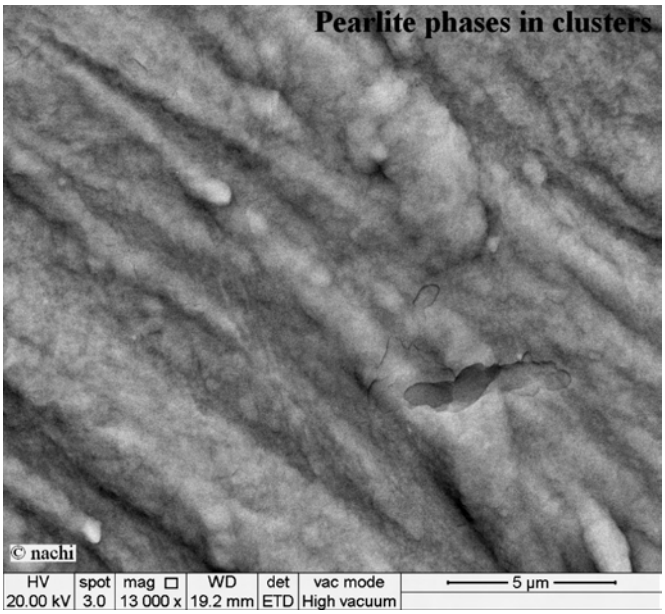

Figure 12. Original grains matrix.

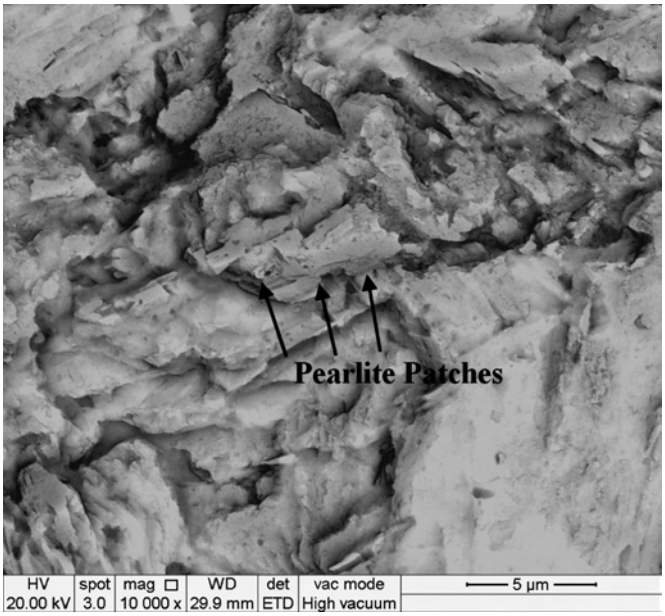

Figure 13. Refined grains matrix.

The energy-disperse x-ray (EDX) detection was conducted to determine the chemical distribution of the base metal at the welded areas in addition to unwelded areas. The results are showing that the carbon content is slightly increased and iron content is slightly reduced due to the phase transformations as how seen in the micro structural views. Figure 15 determines the chemical properties' changes at the fusion zone as compare to

base metal (Fig. 16) for servo based electrode actuation system. This phase changes was the root cause of hardness increment due to solidification process on both system. When the carbon content in the steel is increased, the amount of pearlite increases until it gets the fully pearlitic structure as how seen in the pneumatic system.

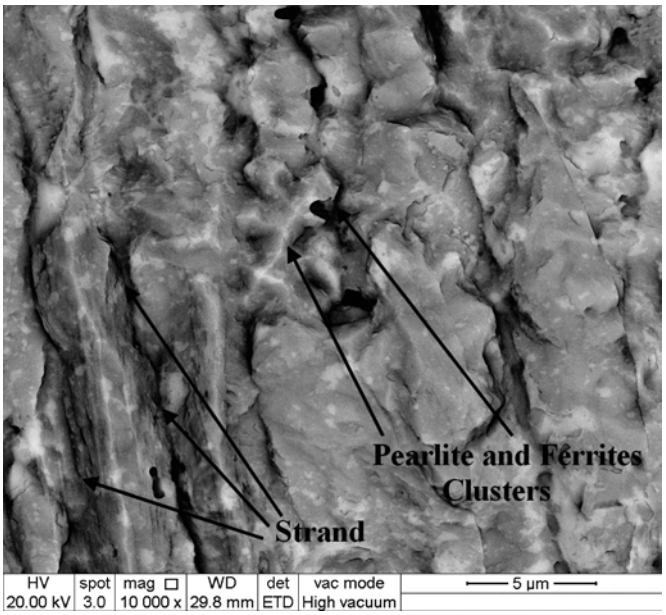

Figure 14. Grain coarsened matrix.

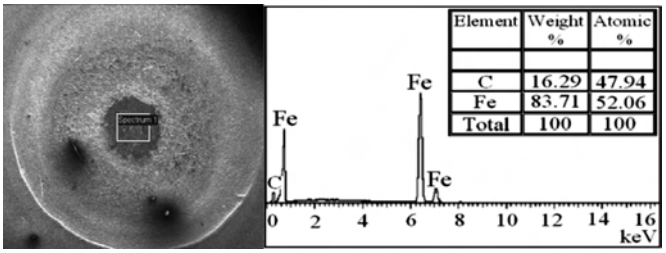

Figure 15. Chemical properties at the fusion zones.

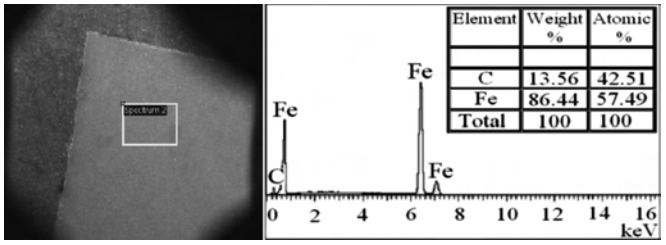

Figure 16. Chemical properties at the base metal.

3.5. Deformation of electrode tips

Hitting the base metals during squeezing cycle is a major problem in pneumatic based electrode actuation system[16-17]. This factor can reduce the lifespan of electrodes caps and also cause fast mushroom growing at the edge of electrode caps or tips. So the electrode caps that involved in the welding process was analysed for both systems. It was found that the servo based system protects the electrode tip geometry from the hitting effect due to smooth touch as compared to the pneumatic based system. Though the electrode tips are cleanable using conventional tip dressers for pneumatic system; the mushrooming effects are still enlarging the diameter tips and resulting resistive drop (contact resistance, $Rc = \rho\ell/A$) during welding process. Here, I have included the photographs of the electrode tips for both electrode actuation systems. Figure 17 shows the electrode tip geometry

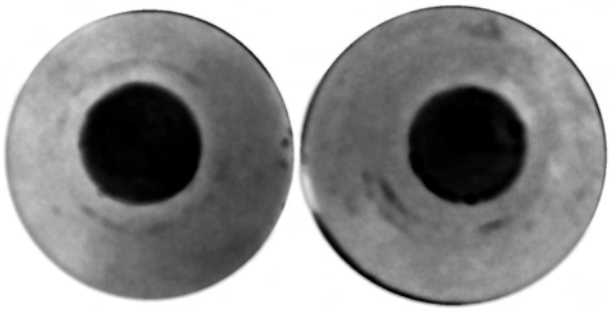

Figure 17. Electrode tips of servo based weld

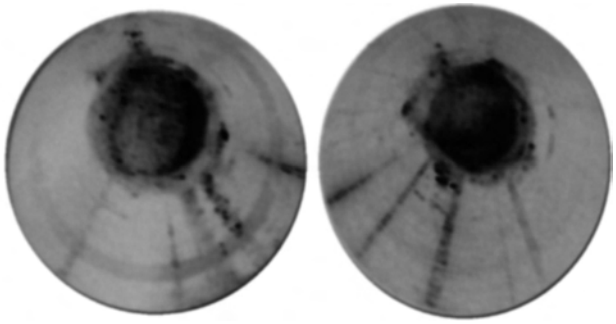

Figure 18. Electrode tips of pnuematic based weld

after 250 welds were made using servo based mechanism while Figure 18 shows the electrode tip geometry after 250 welds were made using pneumatics based system.

4. Conclusion

This experimental investigation looks into the spot weld nugget growth of medium carbon (0.4%) steel using servo based electrode actuation system and it finalizes the facts that: the tensile shear force was slightly higher in the servo based experiment as compared to the pneumatic based experiment (part 1) because of the weld beads diameters increment. The strength increments in terms of percentage were noticed from 11 to 25% upon the parametric variations. A combination of 8 kA, 3 kN and 20 cycles (weld schedule 9) was the highest limit of parameter set up for 1 mm thickness, from which the widest diameter was recorded at 5.899 mm. A combination of 6 kA, 3 kN and 10 cycles was the lowest limit of parameter set up for 1 mm thickness, from which the least acceptable diameter was recorded at 3.676 mm. The common crack initiation and post crack propagation modes that noticed during tensile test was only the PF and TF modes. There was no IF mode appeared at all due to the suppression of forging force fluctuations. The hardness distribution was almost same as the pneumatic based system because the solidification process was same for both systems. Thus, the values were increased from 55 HRB (unwelded areas) to 105 HRB (welded areas) in average as how noticed in the pneumatic system previously. Carbon content was slightly increased at the welded zones but it does not produce profound changes on either hardness or micro structural orientation. Macro structures of BM, FZ and HAZ were remained almost similar to the pneumatic based

system except the diameter of weld beads. The electrode tips' geometries were noticeably affected on the pneumatic based system as compared to the servo based system after 250 welds were made.

Acknowledgement

I would like to thank Ministry of Science, Technology and Innovation, Malaysia (MOSTI) for their financial support during the experimental work. This research outcome is part of Nachimani Charde's doctoral research.

References

[1]. Nachimani, C. (2012). Spot weld growth on medium carbon steel (Part 1). *International Journal of Mechanical and Materials Engineering*, No. 1, Vol. 7, 36–40.
[2]. Aslanlar, S. (2006). The effect of nucleus size on mechanical properties in electrical resistance spot welding of sheets used in automotive industry. *Materials and Design*, 27, 125–131.
[3]. Niu, B. (2009). Improving productivity and quality in automotive spot welding-servo gun based. *Automation and Control*, Vol 2, 120-131.
[4]. Shih, F.L.; Li, X.W; Yoke, R.W and Rung, W. (2010). Input electrical impedance as quality monitoring signature for characterizing resistance spot welding. *NDT&E International*, 43, 200–205
[5]. Darwish, S.M. (2004). Peel and shear strength of spot-welded and weld-bonded dissimilar thickness joints. *Journal of Materials Processing Technology*, Vol. 147, 366-378.
[6]. Pouranvari, M. (2011). Analysis of fracture mode of galvanized low carbon steel resistance spot welds. *International Journal of Multidisciplinary Science and Engineering*, No. 6, Vol. 2, 68-77.
[7]. Rogeon, P. (2008). Characterization of electrical contact conditions in spot welding assemblies. *Journal of Materials Processing Technology*, Vol. 195, 117–124.
[8]. Chein, C.S. (2002). Investigation of monitoring systems for resistance spot welding. *Welding Journal*, 195–199.
[9]. Dickinson, D.W. (1980). Characterization of spot welding behaviour of dynamic electrical parameter monitoring. *Welding Journal*, 170-176.
[10]. Khodabakhshi, F. (2011). Mechanical properties and microstructure of resistance spot welded severely deformed low carbon steel. *Materials Science and Engineering A*, 7, 330-339.
[11]. Mukhopadhyay, G.; Bhattacharya, S.; and Ray, A. (2009). Effect of pre-strain on the strength of spot-welds. *Materials and Design*, 30, 345-354.
[12]. Zhang, X.; Chen, G.; Zhang, Y.; and Lai, X. (2009). Improvement of resistance spot weld ability for dual-phase (dp600) steels using servo gun. *Journal of Materials Processing Technology*, 209, 2671–2675.
[13]. Tang, H. (2002). Forging forces in resistance spot welding. *Journal of Engineering Manufacture (Part B)*, Vol. 216, 957-969.
[14]. Bin, N.; Yong lin, C.; and Hui, Z. (2008). Electrode clamping force regulation of servo gun mounted on resistance spot welding robot. *In Proceedings of the International Conference on Advanced Intelligent Mechatronics IEEE*, China, Oct 2008.
[15]. Bin, N.; Yong lin, C.; and Hui, Z. (2009). Dynamic electrode force control of resistance spot welding robot. *In Proceedings of the International Conference on Robotics and Biomimetic IEEE*, China Sept 2009
[16]. Qiu, R. (2010). Effects of electrode force on the characteristic of magnesium alloy joint welded by resistance spot welding with cover plates. *Materials and Manufacturing Processes*, vol. 7, 1304–1308.
[17]. Bowers, R.J.; Sorensen, C.D and Eagar, T.W. (1990). Electrode geometry in resistance spot welding. *Welding Journal*, 45, 123–129s

Nomenclatures	
C	Carbon
Cu	Copper
Mn	Manganese
P	Phosphorus
S	Sulphur
Si	Silicon
QR	Heat Resistance
I^2	Squared current
T	Welding time in cycle
ρ	Resitivity
ℓ	Length
A	Area
Rc	Contact resistance
Cy	Cycle

Abbreviations	
SEM	Electron Scanning Machine
RWMA	Resistance Welding Manufacturing Alliance
HRB	Rockwell hardness scale 'B'
PID	Proportional Integral Derivate Controller
RPM	Revolution per minute
UTS	Ultimate Tensile Strength
kN	kilo Newton
kA	kilo Ampere
ml	mille litter
kg	kilo gram
FZ	Fusion Zone
HAZ	Heat Affected Zone
BM	Base Metal/Parent Metal
IF	Interfacial Fracture
PF	Partial Fracture
TF	Button Pull-out

The first part of this paper has been published in *International Journal of Mechanical and Materials Engineering (IJMME)*, Vol. 7 (2012), No. 1, 36–40.